Saudi Dental Journal (2021) 33, 944–953

King Saud University

Saudi Dental Journal

www.ksu.edu.sa
www.sciencedirect.com

ORIGINAL ARTICLE

An *in vitro* study on the inhibition and ultrastructural alterations of *Candida albicans* biofilm by zinc oxide nanowires in a PMMA matrix

Constanza Apip [a], Alejandra Martínez [a], Manuel Meléndrez [b], Mariana Domínguez [c], Teresita Marzialetti [d,*], Ricardo Báez [e], Gabriela Sánchez-Sanhueza [f], Andrés Jaramillo [g], Alfonso Catalán [h]

[a] *Oral Prosthetic Rehabilitation Program, Department of Restorative, School of Dentistry, University of Concepción, 1550 Roosevelt, Concepción 4070409, Chile*
[b] *Hybrid Material and Polymer Lab, Department of Materials Engineering, Faculty of Engineering, University of Concepción, Concepción, Chile*
[c] *Department of Microbiology, Faculty of Biological Science, University of Concepción, Casilla 160C, Concepción 4070409, Chile*
[d] *Department of Chemical Engineering, Faculty of Engineering, University of Concepción, 219 Edmundo Larenas, Concepción 4070409, Chile*
[e] *Department of Physics, Faculty of Physical and Mathematical Sciences, University of Concepción, 219 Edmundo Larenas, Concepción 4070409, Chile*
[f] *Department of Restorative Dentistry, School of Dentistry, University of Concepción, 1550 Roosevelt St, Concepción 4070409, Chile*
[g] *Department of Mechanical Engineering, Universidad de La Frontera, 01145 Francisco Salazar, Temuco 4780000, Chile*
[h] *Removable Prosthetics, Department of Restorative Dentistry, School of Dentistry, University of Concepción, 1550 Roosevelt St, Concepción 4070409, Chile*

Received 4 January 2021; revised 29 May 2021; accepted 1 August 2021
Available online 5 August 2021

KEYWORD

C. albicans;
Poly(methyl-methacrylate);
Nanowires;

Abstract *Objectives:* The purpose of this study was (i) to investigate whether nanocomposite poly (methyl-methacrylate)-zinc oxide nanowires (PMMA-ZnO-NWs) have *C. albicans* antibiofilm activity; (ii) to evaluate the interaction between components of the nanocomposites based on PMMA-ZnO-NWs by Raman spectroscopy; and (iii) to assess ultrastructural alterations.

* Corresponding author.
E-mail addresses: capip@udec.cl (C. Apip), almartin@udec.cl (A. Martínez), mmelendrez@udec.cl (M. Meléndrez), mdomingu@udec.cl (M. Domínguez), tmarzialetti@udec.cl (T. Marzialetti), rbaez@udec.cl (R. Báez), gasanchez@udec.cl (G. Sánchez-Sanhueza), andresfelipe.jaramillo@ufrontera.cl (A. Jaramillo).

Peer review under responsibility of King Saud University.

Production and hosting by Elsevier

https://doi.org/10.1016/j.sdentj.2021.08.006

Zinc oxide;
Biofilm;
Ultrastructural alteration

Design: Sixty-eight rectangles (17 PMMA (control) and 51 PMMA–ZnO-NWs (250, 500, 1000 ppm ZnO nanowires) were fabricated. *C. albicans* ATCC 10231 and a *C. albicans* clinical strain were tested. Adherence, biofilm formation and ultrastructural alterations were assessed by transmission electron microscopy. Raman mapping images and spectra were analyzed using main component analysis.

Results: Nanocomposite PMMA-ZnO-NWs inhibited the formation of *C. albicans* biofilms 94% at 1000 ppm and 80% at 500 ppm against both *C. albicans* strains. PMMA-ZnO-NWs induced ultrastructural alterations, including cell wall damage and disorganization of the cytoplasmic membrane, resulting in cell lysis. Raman spectroscopy showed new vibrational modes (300–365–485–600 cm^{-1}) for PMMA and ZnO-NW interactions.

Conclusions: PMMA-ZnO-NWs inhibited *C. albicans* dose-dependent biofilm formation and led to changes in the structures and cell membrane. Raman spectroscopy showed chemical interactions between ZnO-NWs and PMMA, as suggested by the appearance of new bands at 301 and 485 cm^{-1}.

1. Introduction

Candida albicans (*C. albicans*) associated denture stomatitis (DS), is an inflammatory reaction of the palatal and alveolar mucosa underlying dentures (Ramage et al., 2004; Catalán et al., 2008). *C. albicans* produces structured biofilm that are resistant to conventional antifungal therapy (Chandra, et al., 2001; da Silva et al., 2010; Wady et al., 2012; Wisplinghoff et al., 2014). Novel strategies are necessary to combat Candida spp. biofilms infections to improve clinical outcomes. Studies have revealed that dental base resin poly(methyl-methacrylate) (PMMA) has antimicrobial activity and improves mechanical and physical properties when metal nanoparticles (NPs) and oxide-metal-NPs were incorporated in monomers (Z. Li et al., 2016; Cierech et al., 2016a; De Matteis et al., 2019; Rudolf et al., 2020). Nanowires (NWs) have the advantage of reinforcing the matrix due to winding of the polymer chains, increasing their dimensional stability and mechanical properties (Rajaka et al., 2019).

Distinct mechanisms of antimicrobial activity of ZnO nanostructures have been reported. Direct contact with cell wall (CW) results in destruction of cell integrity (Lipovsky et al., 2011; Jalal et al., 2018); the release of Zn^{2+} damages the cell membrane (M. Li et al., 2011); and the production of reactive oxygen species disrupt membrane integrity (Lipovsky et al., 2011; Radhakrishnan, et al., 2018).

Toxicity and interaction of ZnO-NPs and ZnO-NWs with biological systems are still unclear (Pandurangan and Kim, 2015; Alghsham et al., 2019). Studies about cytotoxicity of ZnO-NPs in various mammalian cell lines (Pandurangan and Kim, 2015). Gopikrishnan et al. (2010) revealed that ZnO-NWs exposure in HeLa cells did not significantly induce oxidative stress or cell death. However, Alghsham et al. (2019) demonstrated that exposure to ZnO-NWs may induce distinct inflammatory responses through phagocytic uptake. Rudolf et al. (2020) concluded that the PMMA-ZnO-NPs did not induce direct or indirect cytotoxic effects in L929 cell cultures.

C. albicans alterations caused by ZnO-NPs and ZnO-NWs have shown, using scanning electron microscopy (SEM) and transmission electron microscopy (TEM), collapse of the cell (Jalal et al., 2018; Radhakrishnan, et al., 2018; Hosseini et al., 2018).

Raman spectroscopy (RS) provides information about vibrational and rotational transitions in molecules (Dybal and Krimm, 1990; Wang et al., 2014). RS of ZnO-NWs reveals bands at approximately 103, 383, 442, and 583 cm^{-1} attributed to ZnO in the wurzite phase (Morkoç and Özgür, 2009). PMMA resin is a Raman-active compound with characteristic vibrational bands at 600 cm^{-1} for C—C—O and C—COO stretching, 811 cm^{-1} for C—O—C stretching, 1450 cm^{-1} for C—H in plane bending, and 1728 cm^{-1} for C═O stretching (Wang et al., 2014).

It has been postulated that the incorporation of Ag-NPs into PMMA results in stronger antifungal effects than ZnO-NPs (Anaraki et al., 2017). However, PMMA-Ag-NP have also shown a brown discolouration of PMMA (De Matteis et al., 2019). Rudolf et al. (2020) reported that PMMA-ZnO-NPs had a brighter colour than PMMA.

Therefore, the purpose of this study was (i) to investigate whether nanocomposite poly(methyl-methacrylate)-zinc oxide nanowires (PMMA-ZnO-NWs) have *C. albicans* antibiofilm activity; (ii) to evaluate the interaction between components of the nanocomposites based on PMMA-ZnO-NWs by Raman spectroscopy; and (iii) to assess ultrastructural alterations. We hypothesized 1) the inhibition of *C. albicans* biofilm formation by ZnO-NWs in PMMA was concentration-dependent; 2) the ZnO-NWs interact strongly with the bonds of the PMMA and 3) the PMMA-ZnO-NWs damaged cell membrane.

2. Materials and methods

2.1. Strains and inoculum

C. albicans clinical strain (*C. albicans* CS) from a patient with DS as described by Catalán et al., 2008, and the reference strain ATCC 10231 were used. A strain colony was transferred to 5 mL of Sabouraud broth (Oxoid Ltd., Basingstoke, UK) and cultivated for 18 h at 37 °C. A suspension in RPMI-MOPS 1640 (Sigma, St. Louis, MO, USA) was prepared to adjust the turbidity to 0.5 McFarland standard (equivalent to 1-5 × 10^6 CFU/mL) by Oxoid Turbidimeter (Fisher Scientific Company, Ottawa, Canada).

2.2. Characterization of ZnO-NWs

The morphology of ZnO-NWs was observed by SEM using an FEG Hitachi S-5500 ultrahigh-resolution electron microscope (0.4 nm at 30 kV) with a BF/DF Duo-STEM detector and in a FEI-Nanonova 100 FESEM.

The elemental composition of ZnO-NWs was analyzed by energy dispersive spectrometry (EDS). Samples for EDS were mounted on a carbon-coated copper grid. High-resolution-TEM (HR-TEM) was performed in a JEM-ARM200F probe aberration-corrected analytical microscope with a resolution of 0.08 nm. Selected area electron diffraction was performed using a JEOL 2010F operating at 200 kV (0.19 nm). X-ray diffraction (XRD) was performed using a Philips X'Pert PW3040 diffractometer (PANalytical, Almelo, the Netherlands) with Cu-Ka radiation.

2.3. Nanocomposite's preparation

Sixty-eight rectangular specimens (10 × 5 × 3 mm) were prepared. PMMA specimens without NWs (control) were prepared with thermally polymerized PMMA (MelioDent Heat Cure, Heareus Kulzer, Hanau, Germany). Test specimens were fabricated with ZnO-NWs (25–45 nm thickness), adding 250, 500 ppm, and 1000 ppm (Solis-Pomar et al., 2016). ZnO-NWs were suspended in liquid monomer**.** The acrylic powder was added to the monomer liquid. The specimens were sterilized using UV-irradiation for 20 min (Thermo Fisher Scientific, Waltham, Massachusetts, USA).

2.4. PMMA-ZnO-NWs analysis

Raman analysis was performed using a high-resolution confocal LabRamHR Evolution Horiba Jobin Yvon microscope with a 633-nm edge laser line excitation source (13.3 mW). The laser spot was focused on the specimen using an optic Objective Olympus 100x VIS and NUV camera (B/S UV 50/50 + Lens F125 D25). Raman mapping of a 16 × 16 μm^2 area was performed in each specimen. RS mapping images and spectra were analyzed using multivariate data analysis. All chemometric analysis was performed using MIA-ToolBox and PLS-ToolBox in MATLAB.

2.5. C. albicans adherence and biofilm formation

Adherence and biofilm growth of *C. albicans* ATCC 10231 and *C. albicans* CS were performed according Da Silva et al. (2010), Wady et al. (2012) and Z. Li et al. (2016).

Rectangles were placed inside sterilized 24-well plates for adherence and 32 for biofilm in 96-well plates. Two mL aliquots of *C. albicans* suspensions were added. Plates were incubated at 37 °C for 90 min for the adherence assay and 72 h for biofilm formation in a Litekvo Shaking Incubator (THZ-100, Shanghai, China) at 100 rpm to promote the adherence of *C. albicans* to the surface of PMMA specimens. Cell suspensions were aspirated, and each well was washed twice with 3 mL of sterile PBS to remove non-adhered yeasts. For the biofilm formation assay, the specimens were washed twice with 3 mL of sterile PBS every 24 h for 72 h.

2.6. C. albicans adherence and biofilm formation by SEM

The specimens were fixed overnight at 4 °C in 1 mL of buffer solution containing 2.5% glutaraldehyde. They were post-fixed in 200 μL of 1% OsO_4 for 60 min, dehydrated in ethanol (25, 50, 75, 90, and 100%) and dried in a critical point dryer (Quorum K850, East Sussex, England). The specimens were mounted on metallic stubs, sputter-coated with gold (SPI-Module, Westchester, USA) and examined by SEM (JEOL, JSM 6380 LV, Tokyo, Japan).

2.7. C. albicans analysis by TEM

Cells were collected after being exposed to biofilm experimental conditions and centrifuged (5 min, 5000 rpm). The pellets were fixed in 1 mL of buffer (2.5% glutaraldehyde) overnight at 4 °C. Yeasts were post-fixed for 2 h in OsO_4 containing 1.25% $K_4Fe(CN)_6$ and 5 mM $CaCl_2$ in cacodylate buffer (pH 7.2), washed with the same buffer, dehydrated in ethanol and embedded in Spurr's resin. Ultrathin sections were stained with uranyl acetate and lead citrate. A TEM (JEOL, JEM. 1200 EX II, Tokyo, Japan) and a camera (Gatan Model 17882, Erlangshen ES 500 W, Munich, Germany) were used.

2.8. Biofilm calculation

Biofilm formation was evaluated using SEM images (1000×), and biofilm coverage area (BA) was quantified with ImageJ v.1.47 (National Institute of Health, Bethesda, Maryland, USA). BA was calculated as a percentage as the ratio between the BA formed for each sample and BA in the control sample image.

3. Results

3.1. ZnO-NWs characterization

Fig. 1A shows an SEM micrograph of ZnO-NWs. Fig. 1B presents EDS analysis performed on ZnO-NWs displaying characteristic peaks of Zn(L), Zn(K) and O(K), ZnO-NWs are pure since no metal contamination was detected. The carbon comes from the grid. Fig. 1C displays an HR-TEM micrograph indicating a thickness of 25 nm and preferential growth of the wires in the [0 0 2] direction.

The XRD analysis of ZnO-NWs in Fig. 1D shows typical peaks at 2θ = 31.7°, 33.9°, 36.2°, 47.3°, 56.4°, 62.7° and 67.8° corresponding to planes (1 0 0), (0 0 2), (1 0 1), (1 0 2), and (1 1 0) respectively, which can be indexed to a wurtzite hexagonal ZnO structure in the standard (JCPDS 75-0576) (a = 0.3249 nm, c = 0.5205 nm).

3.2. Raman spectroscopy

Fig. 2 shows the optical field and vibrational spectra of pure PMMA and PMMA-ZnO-NWs (250, 500 and 1000 ppm). The second column shows changes in the distribution of the main component (MC) of PMMA concerning ZnO-NWs concentrations. Non-homogeneous distribution of MC was observed. A strong influence of ZnO-NWs at 500 ppm (Fig. 2H) was observed since the distribution area of the MC

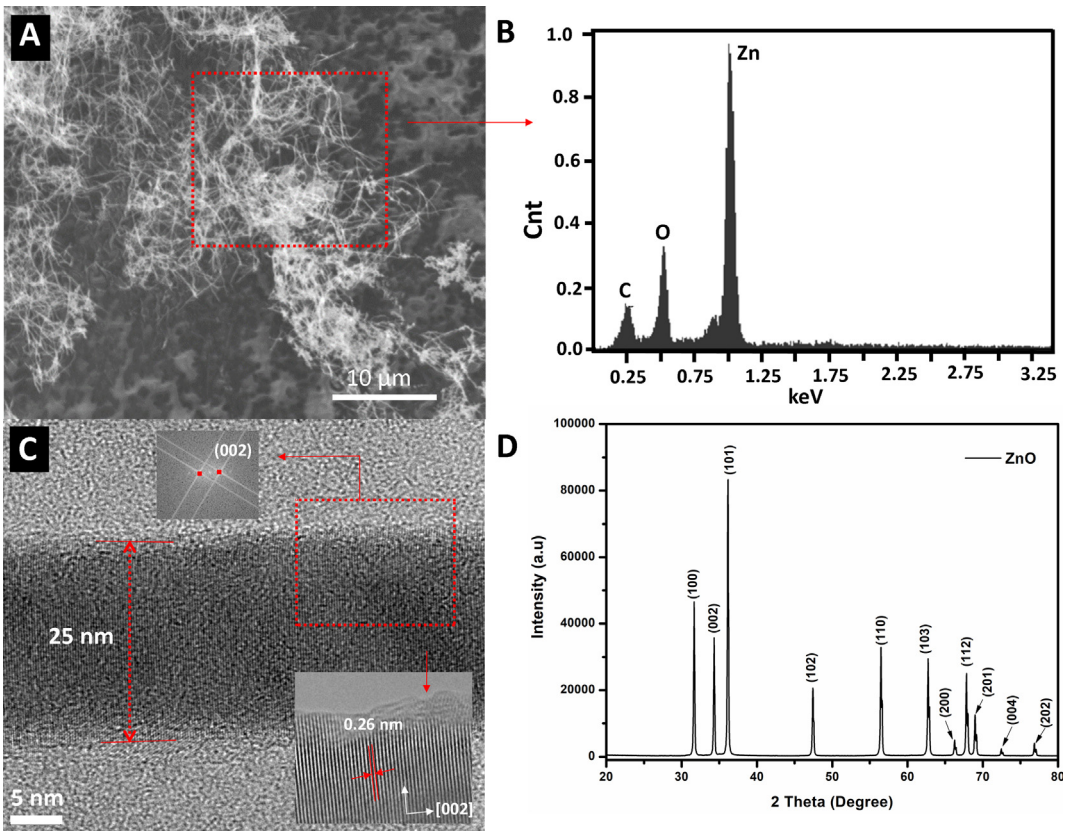

Fig. 1 Characterization of ZnO-NWs. Panel A) SEM micrograph of ZnO-NWs. Panel B) Energy Dispersive Spectrum (EDS) of ZnO-NWs. Panel C) HR-TEM micrograph indicating a thickness of 25 nm and a preferential growth of the wires in the [0 0 2] direction. Panel D) XRD diffractogram of ZnO-NWs.

was minimal for the rest of the specimen. The last column shows RS of each specimen at 0, 250, 500, and 1000 ppm ZnO-NWs, and each spectrum is compared in Fig. 3.

The RS of PMMA and PMMA-ZnO-NWs at different concentrations of ZnO-NWs presented five characteristic vibrational bands in the range of 200 and 2000 cm^{-1}, Fig. 3A. Fig. 3B shows the enhancement of the vibration intensity of each specimen in the region between 200 and 590 cm^{-1}. RS confirmed the characteristic peaks of ZnO-NWs at 300 and 485 cm^{-1}, which were possibly due to the interaction of the oxygen atom of ZnO with the carbons belonging to the carbonyl or ethoxy group of PMMA. The relation between the intensity changes of each peak, 200–590 cm^{-1}, Fig. 3C, which indicates that PMMA-ZnO-NWs at 500 ppm achieved the maximal vibrational intensity of these bonds. Fig. 3D shows the intensity changes of each peak between 200 and 2000 cm^{-1}, in which an exponential increase of the intensity for band at 1453 and 1731 cm^{-1} was observed. The band at 800 cm^{-1} had irregular behavior. The band at 900 cm^{-1} increased gradually until the concentration of ZnO-NWs reached 500 ppm, and then remained almost stationary until the concentration reached 1000 ppm.

3.3. Adherence and biofilm formation by SEM

Fig. 4 shows SEM of *C. albicans* adherence on PMMA and PMMA-ZnO-NWs. The adherence decreased as the concentration of ZnO-NWs on PMMA increased from 250 ppm (Fig. 4B) to 1000 ppm (Fig. 4D).

A mature biofilm, a multilayered network of yeast cells and hyphae embedded in an extracellular matrix, was developed in control (Fig. 5A). PMMA-ZnO-NWs at 250 ppm exhibited a monolayer biofilm and a large amount of polysaccharide (Fig. 5B). PMMA-ZnO-NWs at 500 and 1000 ppm presented small clusters of yeast (Fig. 5C and D).

The BA covered by *C. albicans* ATCC 10231 was 1674 μm^2 (control), for *C. albicans* CS was 2218 μm^2 (control). *C. albicans* CS had 25% more coverage than the ATCC 10231 strain. The percentage of BA on PMMA-ZnO-NWs at 250 ppm was 21% (343 μm^2) and 31% (698 μm^2) for *C. albicans* ATCC 10231 and the clinical strain respectively. At 500 ppm, BA was 334 and 440 μm^2 for *C. albicans* ATCC 10231 and the clinical strain, respectively; their biofilm coverage percentage was 20% for both *C. albicans* strains. At 1000 ppm, BA was 98 and 140 μm^2 for *C. albicans* ATCC 10231 and the clinical strain respectively; the percentage of BA was 6% for both *C. albicans* strains.

The biofilm inhibition percentages were 94 and 80% for both strains at 1000 and 500 ppm PMMA-ZnO-NWs respectively. At 250 ppm the biofilm inhibition was 79% for *C. albicans* 10231 and 69% for the clinical strain.

3.4. C. albicans by SEM and TEM

Fig. 6A-L shows SEM and TEM results of untreated and treated *C. albicans* 10231 with PMMA-ZnO-NWs. Fig. 6A-C control samples; D-F show PMMA-ZnO-NWs at 250 ppm; G-I

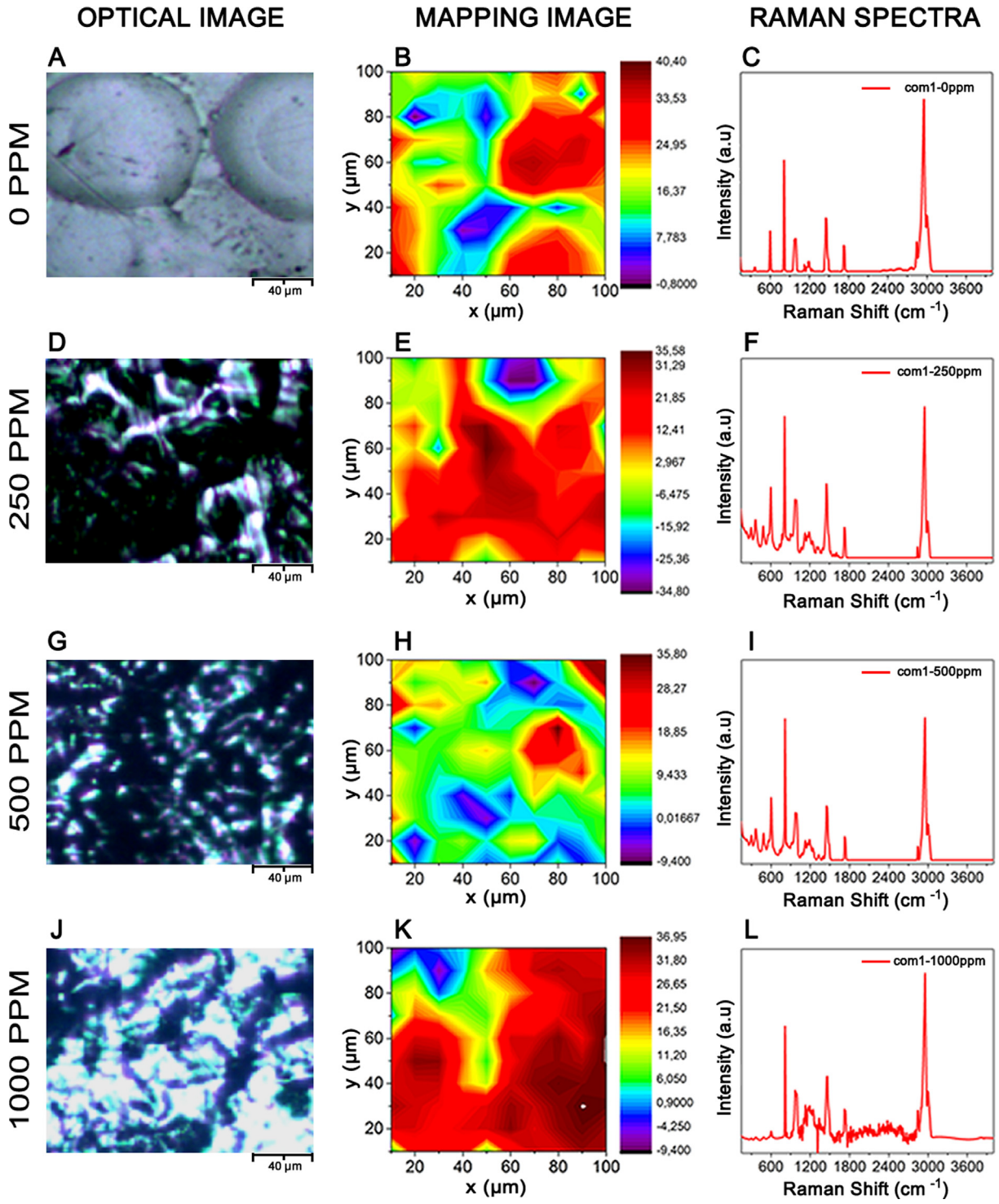

Fig. 2 Images of the optical field, Raman mapping and vibrational spectrum of pure acrylic resin specimen (PMMA) and PMMA–ZnO-NWs at 250, 500 and 1000 ppm of ZnO-NWs. Panels A, D, G and J correspond to optical field images at 100 × 100 μm^2 area; panels B, E, H, and K, represent Raman mapping at 100 × 100 μm^2 area; panels C, F, I and L corresponding to Raman spectrum.

show PMMA-ZnO-NWs at 500 ppm; and J-L show PMMA-ZnO-NWs at 1000 ppm.

SEM of untreated *C. albicans* ATCC 10231 show blastospores and hyphae with intact and smooth CW and normal buds (Fig. 6A). Cells treated with PMMA-ZnO-NWs at 250 ppm had an increased size (Fig. 6D), showing irregular CW. At 500 ppm, *C. albicans* ATCC 10231 showed blastospores and hyphae that were rougher and swollen, cavitation

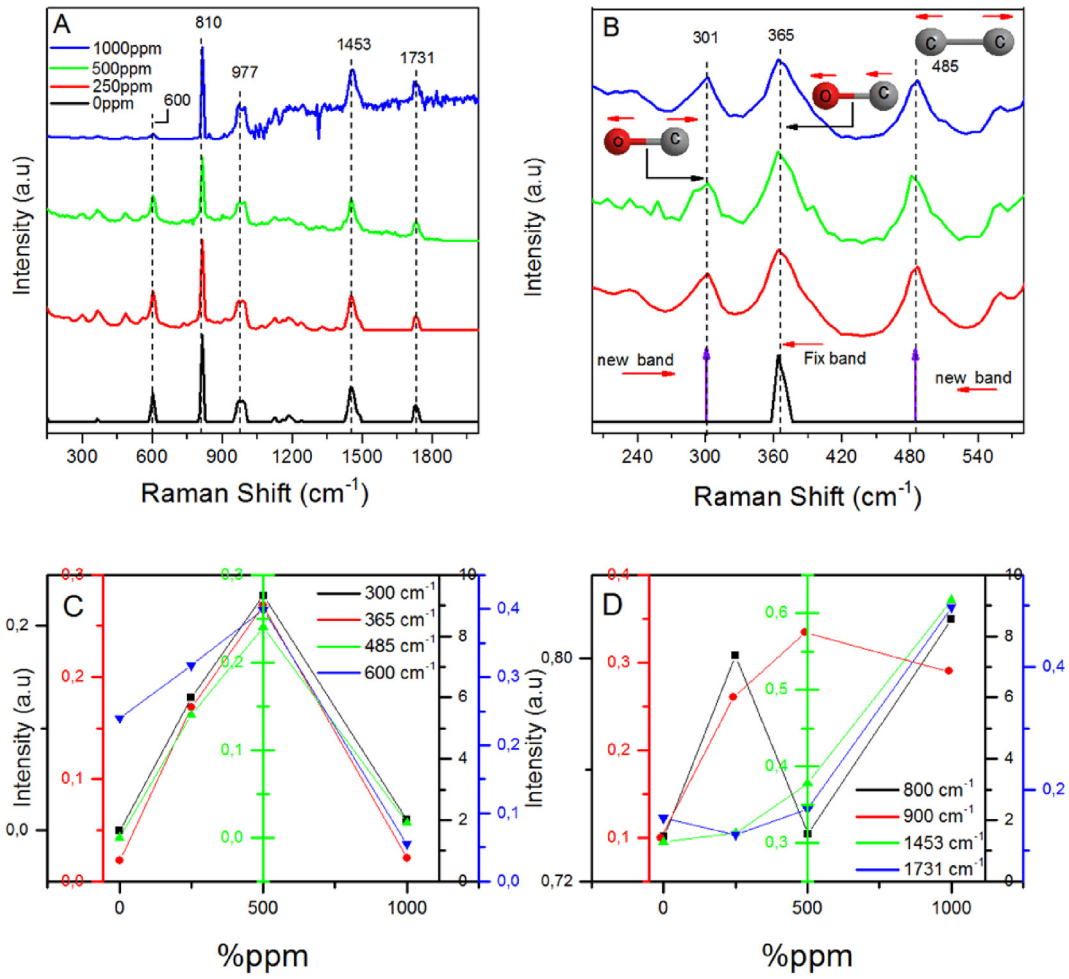

Fig. 3 Raman spectra of PMMA (control) and PMMA–ZnO-NWs at 250, 500, 1000 ppm of ZnO NWs. (A) 200–2000 cm^{-1} region; (B) amplification of 230–590 cm^{-1} region and assignment of main Raman bands; (C) and (D) represent percentage of intensity of the vibrational band at 300, 365, 485 and 600 cm^{-1}, and 800, 900, 1453 and 1731 cm^{-1} respectively.

on the surface of the CW and rings of bud scars located on one side of the hyphal septum (Fig. 6G). Cell damage was observed with large increase in size and irregular morphology (Fig. 6J).

TEM of untreated *C. albicans* ATCC 10231 showed a structured nucleus, cytoplasm with mitochondria, intact cytoplasm membrane and CW (Fig. 6B). A standard CW was formed by several layers having fimbriae (Fig. 6C). Treated yeast with PMMA-ZnO-NWs at 250 ppm exhibited wrinkled CW with loss of the fimbriae and disorganization of the cytoplasmic membrane (Fig. 6E, 6F). At 500 ppm, exhibited disorganized CW causing invagination without CW rupture (Fig. 6H). Yeast cells became distorted with disrupted CW and cytoplasm membrane (Fig. 6I). At 1000 ppm, showed complete collapse with necrosis and invagination of the CW (Fig. 6K). A magnified image of the CW shows a loss of fimbriae and the release of intracellular material leaking (Fig. 6L).

4. Discussion

It has been demonstrated that metal nanomaterials frequently increase antimicrobial activity and reduce toxicity after immobilization in a polymer matrix but also avoid aggregation (Nirmala et al., 2010, Jalal et al., 2018). The incorporation of ZnO-NWs in the PMMA matrix that forms this new nanocomposite could offer sustained release of antimicrobial agents of desirable quality in dentures.

To the author's knowledge, no study has ever reported the anti-*C. albicans* biofilm potential of PMMA-ZnO-NWs; hence, our discussion will focus on comparing PMMA modifications with nanoparticles.

Our results showed that *C. albicans* adherence and biofilm formation considerably decreased with increasing ZnO-NWs concentrations in PMMA-ZnO-NWs, supporting the first hypothesis.

These findings are consistent with other authors (Nam et al., 2012; Cierech et al., 2016a; Z. Li et al., 2016; Anaraki et al., 2017; De Matteis et al., 2019).

In this study, ZnO-NWs were trapped within the PMMA matrix to form PMMA-ZnO-NWs by either physical attachment or chemical bonding. Fig. 3C shows that there is an increase in the peak intensity corresponding to ZnO and PMMA at 500 ppm. A surface-enhanced Raman spectroscopy (SERS) effect occurs between the surface of ZnO and the functional carbon group of the polymer, specifically in the most polar plane of the nanowire [0 0 2], which is the plane of pref-

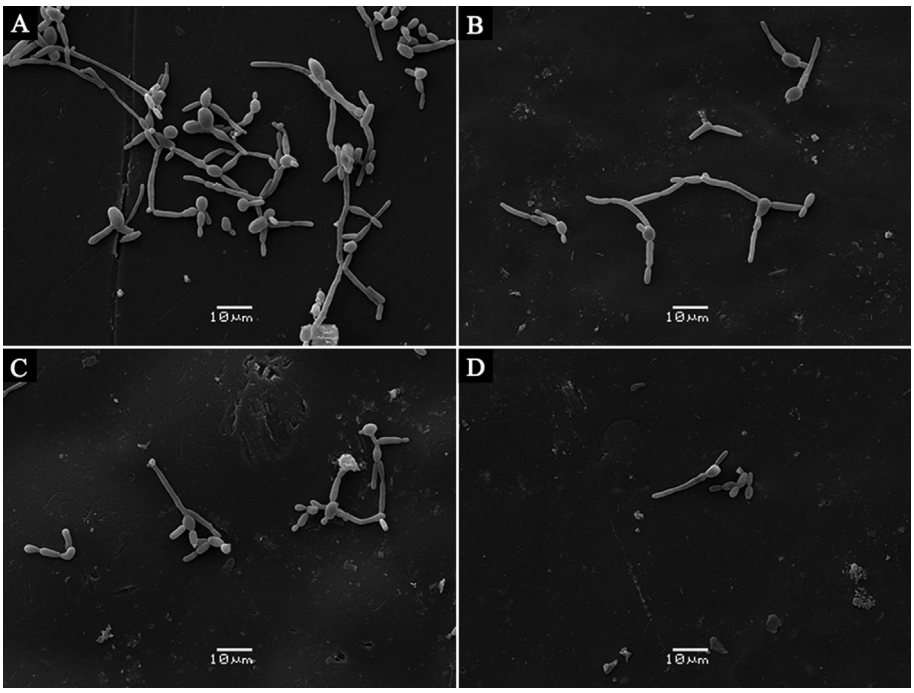

Fig. 4 SEM analysis of *C. albicans* clinical strain following 90 min incubation at 37 °C on acrylic resin PMMA and PMMA–ZnO-NWs. Panel A shows lots of *C. albicans* blastospores and hyphae on the acrylic resin (control). Panel B shows PMMA–ZnO-NWs at 250 ppm having a moderate amount of *C. albicans*. Panel C exhibits PMMA–ZnO-NWs at 500 ppm with few *C. albicans* blastospores and hyphae. Panel D shows PMMA–ZnO-NWs at 1000 ppm having an exiguous amount of *C. albicans*.

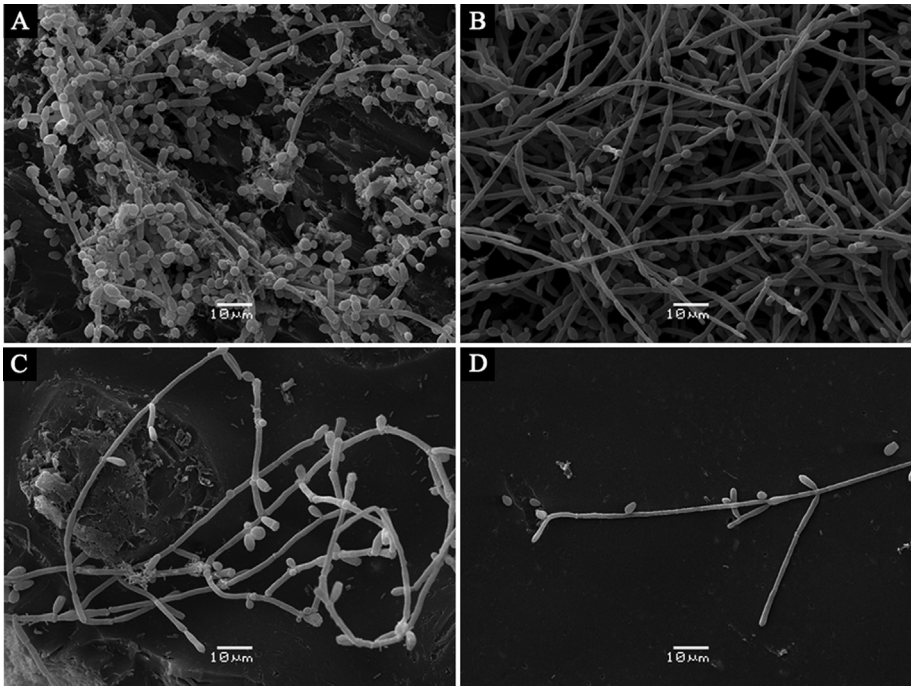

Fig. 5 Representatives SEM images of *C. albicans* clinical strain biofilm formation on PMMA–ZnO-NWs. Panel A represents the control sample exhibiting a dense mature biofilm; the surface shows a predominance of blastospores with some hyphae cells. Panel B evidences biofilm formation on PMMA–ZnO-NWs at 250 ppm with hyphae and few blastospores. Panel C shows an irregular surface of PMMA–ZnO NWs at 500 ppm with scarce biofilm formation. Panel D evidences a considerable decrease in biofilm development on PMMA–ZnO-NWs at 1000 ppm.

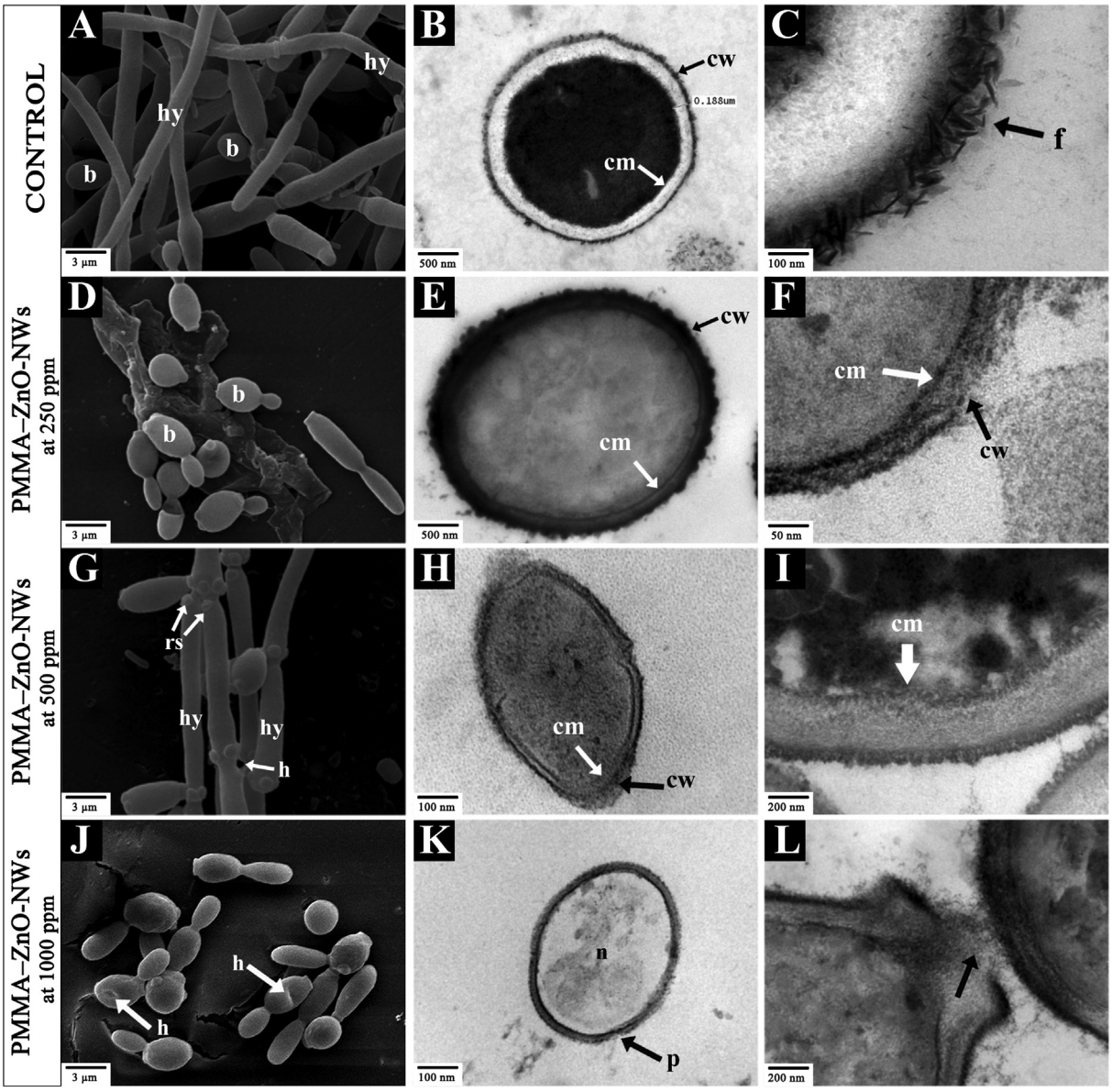

Fig. 6 Representative SEM photographs (left column) and TEM micrographs (central and right column) of *C. albicans* ATCC 10231 incubated for 72 h with PMNA–ZnO-NWs. Panels A-C show untreated cells (Controls). (A) *C. albicans* with normal surface, blastopores (b) and hyphae (hy). (B) *C. albicans* with continuous cytoplasm membrane (cm) and compact cell wall (cw). (C) Intact cell wall with fibrillar structures fimbriae (f). Panels D-F show *C. albicans* treated with PMNA–ZnO-NWs (250 ppm). (D) *C. albicans* presents increasement in cell size and irregularity of the surface. (E) *C. albicans* presents a wrinkled cell wall (cw) and a difusse cytoplasm membrane (cm). (F) The cell wall (cw) and cytoplasm membrane (cm) were damaged. Panels G-I show *C. albicans* treated with PMNA–ZnO-NWs (500 ppm). (F) The cell wall (cw) and cytoplasm membrane (cm) were damaged. (G) *C. albicans* presents increasement in hyphae (hy) size with ring of bud scars (arrows) and holes (h) on the surface. (H) The cell wall of *C. albicans* was perforated (p). (I) *C. albicans* exhibits invaginations of cytoplasm membrane (cm) extending into the cytoplasm. Panels J-L show *C. albicans* treated with PMNA–ZnO-NWs (1000 ppm). (J) *C. albicans* present pits and holes (h) in the cell wall. (K) *C. albicans* shows a complete collapse with necrosis (n) and perforation (p) of cell wall. (L) The arrow shows release of intracellular material.

erential growth. Other vibrational modes are expressed with different intensities at higher wavenumbers due to a higher degree of freedom of the carbonyl and ethoxy groups of PMMA when they do not interact with ZnO (Solis-Pomar et al., 2016). These results agree with those of Cierech et al. (2016b), who characterized ZnO-NPs-PMMA.

The second hypothesis was fully supported by the increase of the bands at 301 and 485 cm^{-1}, evidencing that PMMA had chemical bonds with ZnO-NWs (Özgür et al., 2005); ZnO-NWs may easily be bonded by electron exchange (Alim et al., 2005, Jaramillo et al., 2017). The behavior of the vibration band at 301 cm^{-1} is associated with the average vibration

(bending) of a simple carbon-oxygen bond outside the plane of PMMA (Haris et al., 2010). The band at 485 cm^{-1} for the same specimen is associated with an average vibration between two carbon atoms (Dybal and Krimm, 1990). The decrease in the intensity of vibration corresponding to the bands at 300–36 5–485–600 cm^{-1} with 1000 ppm ZnO-NWs could be associated with the high concentration of ZnO-NWs generating a decrease in the main vibrations of PMMA (Calleja and Cardona, 1977). In contrast, the bands at 1453 and 1731 cm^{-1}, associated with the CH_3 and CO bonds, respectively, were the only bands that had an enhancement of the vibration with increasing concentrations of ZnO-NWs. This observation was associated with a SERS effect (Guzmán-Embús, et al., 2013; Jaramillo et al., 2017).

The third hypothesis that PMMA-ZnO-NWs damage the cell membrane of *C. albicans* was fully supported by SEM and TEM observations. Our results show several ultrastructure alterations, such as abnormal cell morphology, an increase in surface roughness, irregular thickness and rupture of CW, detachment of the cytoplasmic membrane, and destruction of organelles with leakage of the cytoplasm. PMMA-ZnO-NWs at 1000 ppm induced necrosis, as evidenced by the TEM images. These findings agreed with previous reports of *C. albicans* treated with Ag-NPs (Lara et al., 2015; Radhakrishnan et al., 2018), ZnO-NPs (Jalal et al., 2018; Hosseini et al., 2018) and Cu-NWs and Cu-NPs (Martínez et al., 2020).

Among limitations of this study lack evidence of the chemical and physical mechanisms used by the PMMA-ZnO-NWs to kill *C. albicans*. The cytotoxicity of PMMA-ZnO-NWs was not assessed. For clinical application, further studies including colour stability and long-term effects are still required.

5. Conclusions

PMMA-ZnO-NWs inhibit *C. albicans* biofilm formation, and it was dose-dependent. PMMA-ZnO-NWs damages the cell membrane of *C. albicans*.

The appearance of new bands at 301 and 485 cm^{-1} showed chemical interactions between ZnO-NWs and PMMA.

CRediT authorship contribution statement

Constanza Apip: Data curation, Methodology. **Alejandra. Martínez:** Conceptualization, Formal analysis, Validation, Supervision. Writing - original draft, Writing - review & editing. **Manuel F. Meléndrez:** Investigation, Data curation, Methodology, Validation. **Mariana Domínguez:** Methodology, Data curation. **Teresita Marzialetti:** Formal analysis, Writing - review & editing. **Ricardo Báez-Cruz:** Investigation, Data curation, Methodology. **Gabriela Sánchez-Sanhueza:** Data curation, Methodology. **Andrés. Jaramillo:** Data curation, Methodology. **Alfonso Catalán:** Funding acquisition, Resources, Formal analysis, Supervision.

Declaration of Competing Interest

The authors declare that they have no known competing financial interests or personal relationships that could have appeared to influence the work reported in this paper.

Acknowledgment

This work was supported by the Oral Prosthetic Rehabilitation Program, School of Dentistry University of Concepción, Chile.

Authors acknowledge the Laboratory of Nanospectroscopy (LAB-NANOSPECT), University of Concepción, Chile.

We could not forget to mention and celebrate the work and life of our beloved Dr. Alfonso Catalán (R.I.P.). He was, is and will be always an inspiration for us, and the light that guide us through the challenges of research and life. Few times we are able to find those who conjugate the master of his/her arts and the beauty of generosity. He was one of them and we are immensely grateful to have had the chance to meet him.

References

Alghsham, R.S., Satpathy, S.R., Bodduluri, S.R., Hegde, B., Jala, V. R., Waleed Twal, W., Burlison, J.A., Mahendra Sunkara, M., Haribabu, B., 2019. Zinc Oxide Nanowires Exposure Induces a Distinct Inflammatory Response via CCL11-Mediated Eosinophil Recruitment. Front. Immunol. 10, 2604. https://doi.org/10.3389/fimmu.2019.02604.

Alim, K.A., Fonoberov, V.A., Shamsa, M., Balandin, A.A., 2005. Micro-Raman investigation of optical phonons in ZnO nanocrystals. J. Appl. Phys. 97, 124313–124315. https://doi.org/10.1063/1.1944222.

Anaraki, M.R., Jangjoo A., Alimoradi, F., Dizaj S.M., Lotfipour F., 2017. Comparison of Antifungal Properties of Acrylic Resin Reinforced with ZnO and Ag Nanoparticles. Pharm. Sci. 23, 207-214. 10.15171/PS.2017.31

Calleja, J.M., Cardona, M., 1977. Resonant Raman scattering in ZnO. Phys. Rev. B 16 (8), 3753–3761. https://doi.org/10.1103/PhysRevB.16.3753.

Catalán, A., Pacheco, J.G., Martínez, A., Mondaca, M.A., 2008. In vitro and in vivo activity of Melaleuca alternifolia mixed with tissue conditioner on *Candida albicans*. Oral Surgery, Oral Med., Oral Pathol., Oral Radiol. 105 (3), 327–332. https://doi.org/10.1016/j.tripleo.2007.08.025.

Cierech, M., Kolenda, A., Grudniak, A.M., Wojnarowicz, J., Woznіak, B., et al, 2016a. a). Significance of polymethylmetacrylate (PMMA) modification by zinc oxide nanoparticles for fungal biofilm formation. Int. J. Pharm. 510, 323–335. https://doi.org/10.1016/j.ijpharm.2016.06.052.

Cierech, M., Wojnarowicz, J., Szmigiel, D., Baczkowski, B., Grudniak, A., Wolska, K., Łojkowski, W., Mierzwinska-Nastalska, E., 2016b. Preparation and characterization of ZnO-PMMA resin nanocomposites for denture bases. Acta Bioeng. Biomech. 18, 31–41. https://doi.org/10.5277/ABB-00232-2014-04

Chandra, J., Mukherjee, P., Leidich, S., Faddoud, F., Hoyer, L., Douglas, L., et al., 2001. Antifungal resistance of candidal biofilms formed on denture acrylic in vitro. J. Dental Res. 80, 903-8. https://doi.org/10.1177/00220345010800031101

da Silva, W.J., Seneviratne, J., Samaranayake, L.P., Del Bel Cury, A. A., 2010. Bioactivity and architecture of *Candida albicans* biofilms developed on poly (methyl methacrylate) resin surface. J. Biomed. Mater. Res. 94, 149–156. https://doi.org/10.1002/jbm.b.31635.

De Matteis, V., Cascione, M.F., Toma, C.C., Albanese, G., De Giorgi, M.L., Corsalini, M., Rinaldi, R., 2019. Silver Nanoparticles Addition in Poly(Methyl Methacrylate) Dental Matrix: Topographic and Antimycotic Studies. Int. J. Mol. Sci. 20, 4691–4705. https://doi.org/10.3390/ijms20194691.

Dybal, J., Krimm, S., 1990. Normal-mode analysis of infrared and Raman spectra of crystalline isotactic poly (methyl methacrylate).

Macromolecules 23 (5), 1301–1308. https://doi.org/10.1021/ma00207a013.

Gopikrishnan, R., Zhang, K., Ravichandran, P., Baluchamy, S., Ramesh, V., Biradar, S., Ramesh, P., Pradhan, J., Hall, J.C., Pradhan, A.K., et al, 2010. Synthesis, characterization and biocompatibility studies of zinc oxide (ZnO) nanorods for biomedical application. Nano-Micro Letters 2, 31–36. https://doi.org/10.5101/nml.v2i1.p31-36.

Guzmán-Embús, D.A., Orrego, Cardozo, M., Vargas-Hernández, C., 2013. Genomic DNA characterization of pork spleen by Raman spectroscopy. J. Appl. Phys. 114, 194704-8. https://doi.org/10.1063/1.4831948

Haris, M.R.H.M., Kathiresan, S., Mohan, S., 2010. FT-IR and FT-Raman spectra and normal coordinate analysis of poly methyl methacrylate. Der Pharma Chem. 2, 316–323.

Hosseini, S.S., Ghaemi, E., Koohsar, F., 2018. Influence of ZnO nanoparticles on *Candida albicans* isolates biofilm formed on the urinary catheter. Iran J. Microbiol. 10, 424–432. http://doi.org/ijm.tums.ac.ir.

Jalal, M., Ansari, M.A., Ali, S.G., Khan, H.M., Rehman, S., 2018. Anticandidal activity of bioinspired ZnO NPs: effect on growth, cell morphology and key virulence attributes of Candida species. Artif. Cells Nanomed. Biotechnol. 46 (sup1), 912–925. https://doi.org/10.1080/21691401.2018.1439837.

Jaramillo, A.F., Baez-Cruz, R., Montoya, L.F., Medinam, C., Pérez-Tijerina, E., Salazar, F., Rojas, D., Melendrez, M.F., 2017. Estimation of the surface interaction mechanism of ZnO nanoparticles modified with organosilane groups by Raman Spectroscopy. Ceram. Int. 43 (15), 11838–11847. https://doi.org/10.1016/j.ceramint.2017.06.027.

Lara, H.H., Romero-Urbina, D.G., Pierce, C., Lopez-Ribot, J.L., Arellano-Jiménez, M.J., Jose-Yacaman, M., 2015. Effect of silver nanoparticles on Candida albicans biofilms: An ultrastructural study. J. Nanobiotechnol. 13, 1–12. https://doi.org/10.1186/s12951-015-0147-8

Li, M., Zhu, L., Lin, D., 2011. Toxicity of ZnO nanoparticles to Escherichia coli: mechanism and the influence of medium components. Environ. Sci. Technol. 45 (5), 1977–1983. https://doi.org/10.1021/es102624t.

Li, Z., Sun, J., Lan, J., Qi, Q., 2016. Effect of a denture base acrylic resin containing silver nanoparticles on *Candida albicans* adhesion and biofilm formation. Gerodontology 33 (2), 209–216. https://doi.org/10.1111/ger.2016.33.issue-210.1111/ger.12142.

Lipovsky, A., Nitzan, Y., Gedanken, A., Lubart, R., 2011. Antifungal activity of ZnO nanoparticles-the role of ROS mediated cell injury. Nanotech 22, 101–105. https://doi.org/10.1088/0957-4484/22/10/105101.

Martínez, A., Apip, C., Melendrez, M.F., Dominguez, M., Sánchez-Sanhueza, G., Marzialetti, T., Catalán, A., 2020. Dual antifungal activity against *Candida albicans* of copper metallic nanostructures and hierarchical copper oxide marigold-like nanostructures grown in situ in the culture medium. J. Appl. Microbiol. 130, 1883–1892 https://doi:10.1111/jam.14859.

Morkoç, H., Özgür, Ü., 2009. Zinc Oxide: Fundamentals, Materials and Device Technology. Wiley-VCH Verlag GmbH & Co, KGaA, Weinheim.

Nam, K.Y., Lee, C.-H., Lee, C.-J., 2012. Antifungal and physical characteristics of modified denture base acrylic incorporated with silver nanoparticles. Gerodontology 29, e413–e419. https://doi.org/10.1111/j.1741-2358.2011.00489.x.

Nirmala, R., Nam, K.T., Park, D.K., Woo-il, B., Navamathavan, R., Kim, H.Y., 2010. Structural, thermal, mechanical and bioactivity evaluation of silver-loaded bovine bone hydroxyapatite grafted poly(ε-caprolactone) nanofibers via electrospinning. Surf. Coat. Technol. 205, 174-181. https://doi.org/10.1016/j.surfcoat.2010.06.027

Özgür, Ü., Alivov, Y.I., Liu, C., Teke, A., Reshchikov, M., Doğan, S., Morkoç, H., 2005) A comprehensive review of ZnO materials and devices. J. Appl. Phys. 98, 041301 1-103. https://doi.org/10.1063/1.1992666

Pandurangan, M., Hwan Kim, D., 2015. In vitro toxicity of zinc oxide nanoparticles: a review. J. Nanopart. Res. 17, 158–166. https://doi.org/10.1007/s11051-015-2958-9.

Radhakrishnan, V.S., Mudiam, M.K.R., Kumar, M., Dwivedi, S.P., Singh, S.P., Prasad, T., 2018. Silver nanoparticles induced alterations in multiple cellular targets, which are critical for drug susceptibilities and pathogenicity in fungal pathogen (*Candida albicans*). Int. J. Nanomed. 13, 2647–2663. https://doi.org/10.2147/IJN.S150648.

Ramage, G., Tomsett, K., Wickers, B.L., López, Ribot, J., Redding, S. W., 2004. Denture stomatitis: a role for Candida biofilms. Oral Surgery, Oral Med., Oral Pathol. Oral Radiol. Endod, 98, 53-59. https://doi.org/10.1016/j.tripleo.2003.04.002

Rajak, D.K., Pagar, D.D., Kumar, R., Pruncu, C.I., 2019. Recent progress of reinforcement materials: acomprehensive overview of composite materials. J. Mater. Res. Technol. 8 (6), 6354–6374. Available online at www.sciencedirect.com.

Rudolf, R., Popović, D., Tomić, S., Bobovnik, R., Lazić, V., Majerič, P., Anžel, I., Čolić, M., 2020. Microstructure Characterisation and Identification of the Mechanical and Functional Properties of a New PMMA-ZnO Composite. Materials 13 (12), 2717. https://doi.org/10.3390/ma13122717.

Solis-Pomar, F., Jaramillo, A., Medina, C., Rojas, D., Mera, A.C., Meléndrez, M.F., E. Pérez–Tijerina, E., 2016. Rapid Synthesis and Photocatalytic Activity of ZnO Nanowires Obtained Through Microwave-Assisted Thermal Decomposition. Ceram. Int. 42, 18045-18052. https://doi.org/10.1016/j.ceramint.2016.08.084

Wady, A.F., Machado, A.L., Zucolotto, V., Zamperini, C.A., Berni, E., Vergani, C.E., 2012. Evaluation of *Candida albicans* adhesion and biofilm formation on a denture base acrylic resin containing silver nanoparticles. J. Appl. Microbiol. 112, 1163–1172. https://doi.org/10.1111/j.1365-2672.2012.05293.x.

Wang, R., Tao, J., Yu, B., Dai, L., 2014. Characterization of multiwalled carbon nanotube-polymethyl methacrylate composite resins as denture base materials. J. Prosthet. Dent. 111 (4), 318–326. https://doi.org/10.1016/j.prosdent.2013.07.017.

Wisplinghoff, H., Ebbers, J., Geurtz, L., Stefanik, D., Major, Y., Edmond, M.B., Wenzel, R.P., Seifert, H., 2014. Nosocomial bloodstream infections due to Candida spp. in the USA: species distribution, clinical features and antifungal susceptibilities. Int. J. Antimicrob. Agents 43 (1), 78–81. https://doi.org/10.1016/j.ijantimicag.2013.09.005.